Studying the limits of production rate and yield for the volume manufacturing of hollow core photonic band gap fibers

Gregory T. Jasion,[1,*] Eric Numkam Fokoua,[1] John S. Shrimpton,[2] David J. Richardson,[1] and Francesco Poletti[1]

[1]*Optoelectronics Research Centre, University of Southampton, Southampton, SO17 1ST, UK.*
[2]*Faculty of Engineering and the Environment, University of Southampton, Southampton, SO17 1ST, UK.*
*g.jasion@soton.ac.uk

Abstract: Hollow core photonic band gap fibers have great potential in low latency data transmission and power delivery applications, but they are currently only fabricated in research scale fabrication facilities, with km-scale lengths. To drive cost reduction and volume manufacturing it is essential to be able to upscale the preform size, but before embarking on costly experimental attempts it is useful to apply fluid dynamics models to study how the fiber drawing dynamics would be affected by such a change. In this work we use a fluid dynamics model to virtually draw increasingly longer lengths of the same fiber from preforms of identical length but different diameters. Taking advantage of our fast numerical model we explore the physical dynamics of the draw process. We discover that the draw tension is the key thermodynamic parameter and that an upper length limit exists beyond which undesirable distortions in the microstructure become difficult to control. These mechanisms are identified and possible mitigation methods described which could allow the fabrication of over 200 km fiber from a single preform.

OCIS codes: (000.4430) Numerical approximation and analysis; (060.2280) Fiber design and fabrication; (060.4005) Microstructured fibers; (060.5295) Photonic crystal fibers.

References and links

1. D. G. Ouzounov, F. R. Ahmad, D. Müller, N. Venkataraman, M. T. Gallagher, M. G. Thomas, J. Silcox, K. W. Koch, and A. L. Gaeta, "Generation of megawatt optical solitons in hollow-core photonic band-gap fibers," Science **301**, 1702–1704 (2003).
2. F. Poletti, N. V. Wheeler, M. N. Petrovich, N. Baddela, E. Numkam Fokoua, J. R. Hayes, D. R. Gray, Z. Li, R. Slavík, and D. J. Richardson, "Towards high-capacity fibre-optic communications at the speed of light in vacuum," Nat. Photonics **7**, 279–284 (2013).
3. P. J. Roberts, F. Couny, H. Sabert, B. J. Mangan, D. P. Williams, L. Farr, M. W. Mason, A. Tomlinson, T. A. Birks, J. C. Knight, and P. J. Russel, "Ultimate low loss of hollow-core photonic crystal fibres," Opt. Express **13**, 236–244 (2005).
4. F. Poletti, M. N. Petrovich, and D. J. Richardson, "Hollow-core photonic bandgap fibers: technology and applications," Nanophotonics **2**, 315–340 (2013).
5. C. M. Smith, N. Venkataraman, M. T. Gallagher, D. Müller, J. A. West, N. F. Borrelli, D. C. Allan, and K. W. Koch, "Low-loss hollow-core silica/air photonic bandgap fibre," Nature **424**, 657–659 (2003).
6. R. Amezcua-Correa, N. G. Broderick, M. N. Petrovich, F. Poletti, and D. J. Richardson, "Optimizing the usable bandwidth and loss through core design in realistic hollow-core photonic bandgap fibers," Opt. Express **14**, 7974–7985 (2006).

7. V. A. J. M. Sleiffer, Y. Jung, N. K. Baddela, J. Surof, M. Kuschnerov, V. Veljanovski, J. R. Hayes, N. V. Wheeler, E. R. Numkam Fokoua, J. P. Wooler, D. R. Gray, N. H. L. Wong, F. R. Parmigiani, S. U. Alam, M. N. Petrovich, F. Poletti, D. J. Richardson, and H. de Waardt, "High capacity mode-division multiplexed optical transmission in a novel 37-cell hollow-core photonic bandgap fiber," J. Lightwave Technol. **32**, 854–863 (2014).
8. B. J. Mangan, M. kuschnerov, J. W. Nicholson, J. Fini, L. Meng, R. Windeler, E. Monberg, A. Desantolo, and V. Mikhailov, "First demonstration of hollow-core fiber for intra data center low latency connectivity with a commercial 100gb/s interface," in "Optical Fiber Communication Conference," (Optical Society of America, 2015), p. M3D.4.
9. Z. Liu, Y. Chen, Z. Li, B. Kelly, R. Phelan, J. O'Carroll, T. Bradley, J. P. Wooler, N. V. Wheeler, A. M. Heidt, T. Richter, C. Schubert, M. Becker, F. Poletti, M. N. Petrovich, S. U. Alam, D. J. Richardson, and R. Slavík, "High-capacity directly modulated optical transmitter for 2-μm spectral region," J. Lightwave Technol. **33**, 1373–1379 (2015).
10. Y. Chen, Z. Liu, S. R. Sandoghchi, G. T. Jasion, T. Bradley, E. Numkam Fokoua, J. Hayes, N. V. Wheeler, D. R. Gray, B. J. Mangan, R. Slavik, F. Poletti, M. Petrovich, and D. J. Richardson, "Demonstration of an 11km hollow core photonic bandgap fiber for broadband low-latency data transmission," in "Optical Fiber Communication Conference Post Deadline Papers," (Optical Society of America, 2015), p. Th5A.1.
11. Z. Yin and Y. Jaluria, "Neck down and thermally induced defects in high-speed optical fiber drawing," J. Heat Transf. **122**, 351–362 (2000).
12. Z. Wei, K.-M. Lee, S. W. Tchikanda, Z. Zhou, and S.-P. Hong, "Free surface flow in high speed fiber drawing with large-diameter glass preforms," J. Heat Transf. **126**, 713–722 (2004).
13. H. Turunen, "Mechanical reliability of optical fiber in combined continuous draw and proof testing process," Phd thesis, Helsinki University of Technology (2005).
14. G. T. Jasion, F. Poletti, J. S. Shrimpton, and D. J. Richardson, "Volume manufacturing of hollow core photonic band gap fibers: Challenges and opportunities," in "Optical Fiber Communication Conference," (Optical Society of America, 2015), p. W2A.37.
15. G. T. Jasion, J. S. Shrimpton, Y. Chen, T. Bradley, D. J. Richardson, and F. Poletti, "Microstructure element method (MSEM): viscous flow model for the virtual draw of microstructured optical fibers," Opt. Express **23**, 312–329 (2015).
16. A. D. Fitt, K. Furusawa, T. M. Monro, C. P. Please, and D. J. Richardson, "The mathematical modelling of capillary drawing for holey fibre manufacture," J. Eng. Math. **43**, 201–227 (2002).
17. E. Numkam Fokoua, D. J. Richardson, and F. Poletti, "Impact of structural distortions on the performance of hollow-core photonic bandgap fibers," Opt. Express **22**, 2735–2744 (2014).
18. E. Numkam Fokoua, S. R. Sandoghchi, Y. Chen, G. T. Jasion, N. V. Wheeler, N. K. Baddela, J. R. Hayes, M. N. Petrovich, D. J. Richardson, and F. Poletti, "Accurate modelling of fabricated hollow-core photonic bandgap fibers," Opt. Express **23**, 23117–23132 (2015).
19. Y. Chen and T. A. Birks, "Predicting hole sizes after fibre drawing without knowing the viscosity," Opt. Mater. Express **3**, 346–356 (2013).
20. Y. M. Stokes, P. Buchak, D. G. Crowdy, and H. Ebendorff-Heidepriem, "Drawing of micro-structured fibres: circular and non-circular tubes," J. Fluid Mech. **755**, 176–203 (2014).
21. P. K. Bachmann, W. Hermann, H. Wehr, and D. U. Wiechert, "Stress in optical waveguides. 2: Fibers," Appl. Opt. **26**, 1175–1182 (1987).
22. H. Schonhorn, H. N. Vazirani, and H. L. Frisch, "Relationship between fiber tension and drawing velocity and their influence on the ultimate strength of laser drawn silica fibers," J. Appl. Phys. **49**, 3703–3706 (1978).
23. P. L. Chu and T. Whitbread, "Measurement of stresses in optical fiber and preform," Appl. Opt. **21**, 4241–4245 (1982).
24. K. Tsujikawa, K. Tajima, and M. Ohashi, "Rayleigh scattering reduction method for silica-based optical fiber," J. Lightwave Technol. **18**, 1528–1532 (2000).

1. Introduction

Hollow core photonic band gap fibers (HC-PBGFs) have ultra low non-linearity [1], low latency [2] and potential for ultralow loss [3, 4], which make them potential contenders for some data transmission applications, as well as excellent candidates for gas sensing and metrology applications requiring compact gas cells with a large overlap between light and gas.

To date HC-PBGFs have been the subject of extensive research focusing, amongst others, on loss reduction, bandwidth optimization and control of modal content [5–7]. These research led activities have so far required only short lengths of fiber, typically less or around the km scale. More recently, driven by acute interest in low-latency data-center applications, a demand for multi-kilometer lengths of HC-PBGFs has arisen, culminating in the fabrication of 2.75 km,

3.8 km and very recently 11 km single spans of fibers through which data was successfully transmitted [8–10]. Regardless of the application, whether it is for meter long devices, for intra or inter data center data transmission, or for longer haul telecoms, these yields of a few kilometer per preform are still orders of magnitude shorter than those achieved for state-of-the-art conventional fibers. For the HC-PBGF technology to stand a chance to impact large volume markets, large quantities of fibers need to be produced at high speed to lower the production costs.

However, the fabrication of HC-PBGF has been limited so far to research-scale environments that use short drawing towers and small bore furnaces, and little is known about the viability and methodology to produce lengths of fibers of the order of hundreds of kilometers from a single preform. In contrast, the fabrication of long lengths of solid fibers has been studied and optimized for decades [11–13] and modern production rates are now in excess of 1.5 km/min, with single preforms able to produce over 1000 km of fiber [13]. While some of the challenges involved in drawing solid and hollow core fibers are similar, the precise control of the internal microstructure in HC-PBGFs poses new challenges which are not present in solid fiber manufacture.

In this paper we use a recently introduced fluid dynamics model to simulate the draw of the same target HC-PBGF from a set of structurally identical holey preforms, homothetically scaled to produce fiber yields ranging from 5 to 500 km per preform. We will first briefly summarize the numerical model we use, then describe the preforms and fibers that will be simulated, and finally identify the physical changes, fluid dynamics-driven, that pose an upper bound to the longest length of good fiber that can be achieved from a single preform. We will conclude by proposing ways to push back those limitations through improvements in preform or fiber design and draw processes. This work builds on a preliminary investigation presented in [14].

2. Numerical model

The MicroStructure Element Method (MSEM) [15] is a numerical fluid dynamics based model that solves the 2D fiber cross-section geometry over the draw. The MSEM is much quicker than finite element methods because it does not resolve the finest features, instead the microstructure is discretized into a network of struts and nodes. Forces of gas pressure, surface tension and viscosity are found on each of those struts and the scheme evolves the position of the nodes to find an equilibrium at each longitudinal position along the neck of the preform inside the furnace. For any given set of drawing parameters (feed speed, draw speed, furnace profile and peak temperature) the shape and temperature profile of the outer glass jacket is solved using a model from Fitt et al. [16]: these are used as the external boundary conditions that drive the evolution of the inner microstructure.

The production of HC-PBGF differs from solid fibers in several ways, the most important being the split of the draw in two stages and the need to apply gas pressure during the second stage draw to prevent hole collapse, Fig. 1. Two gas pressures, independently controlling the core and the whole of the cladding, are typically required in order to oppose surface tension and achieve the desired structure. It is this fundamental difference and the associated draw dynamics that makes upscaling these fibers a more challenging task than for all solid fibers.

3. Volume upscaling

In this section we select a target fiber and launch a series of MSEM simulations to study the problems that might arise when the yield of the preform is increased. We use a range of geometrically similar preforms with the same length (1 m) but different cross-sectional scale to target a fiber with the same cross-section but in lengths ranging from 5 km to 500 km, Table 1. The cladding pitch and thickness in the preforms were chosen so that each fiber had the same

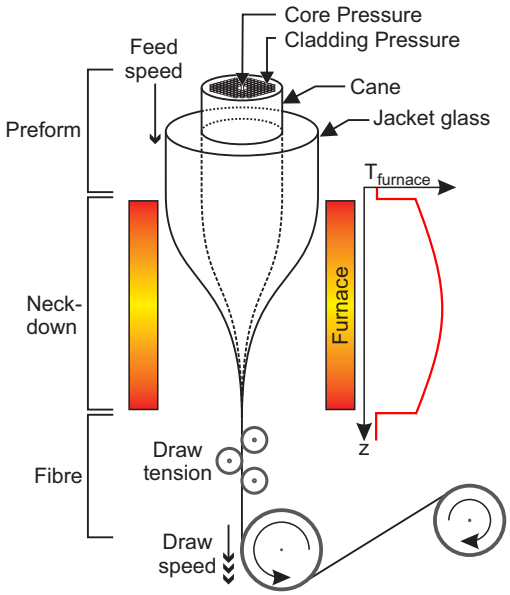

Fig. 1. Illustration of the second stage draw process of HC-PBGF; identifying the two components of the preform, cane and jacket, and the most important control parameters: core and cladding pressures, feed and draw speeds, draw tension (after coating), and furnace temperature and profile.

Table 1. Dimensions of the preforms for each yield. Cane ID and Jacket OD scale with the square root of the yield, production rate scales linearly with yield.

Yield	Cane		Jacket		Production rate	
km	ID/mm	OD/mm	ID/mm	OD/mm	km / h	m/s
5	1.5	1.9	1.9	10.7	0.45	0.125
10	2.1	2.5	2.5	15.2	0.9	0.25
20	3.0	3.4	3.4	21.4	1.8	0.5
30	3.7	4.1	4.1	26.3	2.7	0.75
40	4.2	4.6	4.6	30.3	3.6	1
50	4.7	5.1	5.1	33.9	4.5	1.25
60	5.2	5.6	5.6	37.2	5.4	1.5
100	6.7	7.1	7.1	48.0	9.0	2.5
200	9.5	9.9	9.9	67.8	18	5
300	11.6	12.0	12.0	83.1	27	7.5
400	13.4	13.8	13.8	95.9	36	10
500	15.0	15.4	15.4	107.2	45	12.5

unit cell area in the cladding, and since they all have the same ID and OD they therefore have the same nominal strut thickness. The same feed speed is used, requiring the same total draw time for all fibers but with draw speeds that increase linearly with yield.

Of all the possible target fibers we chose to simulate a HC-PBGF that has recently been produced in a record long length of 11 km [10], Fig. 2(a). Whilst the loss of the fiber ($\approx$5 dB/km) is not the lowest ever reported for these structures, and over one order of magnitude higher than what simulations indicate could be reasonably achievable with improved designs,

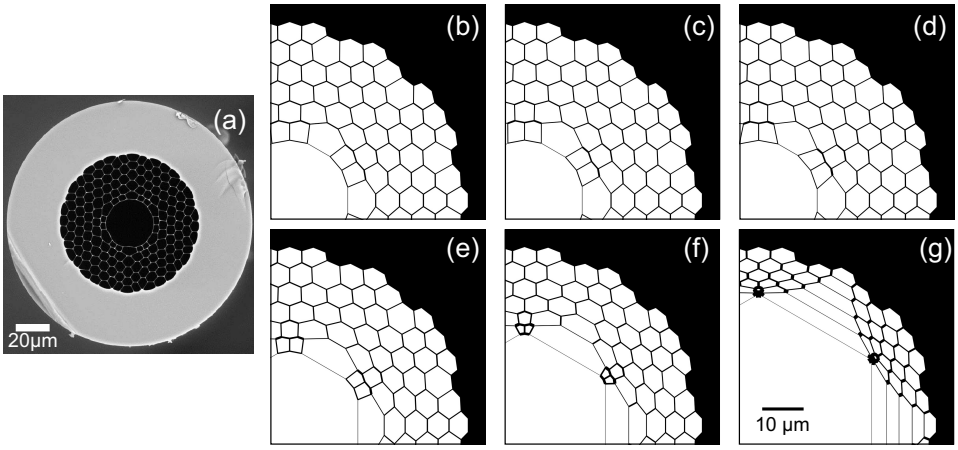

Fig. 2. (a) Scanning Electron Micrograph of experimental fiber from [10]. Microstructure of simulated fibers drawn from preforms in Table 1 with yields: (b) 5 km, (c) 20 km, (d) 50 km, (e) 100 km, (f) 200 km, (g) 500 km.

we believe the conclusions of the study are quite general and could be applied to any other low loss structures as well. The target fiber has 5 rings of capillaries around a core of 19 excluded cells (5 missing capillaries along the diameter). Each fiber is drawn to an outer diameter (OD) of 173 μm and an inner diameter (ID) of the solid jacket of 87 μm, with a targeted average pitch of 5.8μm and a cell diameter to pitch ratio of $d/\Lambda = 0.99$ (as in the fabricated fiber), producing fibers guiding at telecoms wavelengths (between 1200 and 1600 nm). The feed speed is 1.5 mm/s. Setting a target OD and ID uniquely identifies for each fiber the required draw speed, u_d, and cladding pressure, P_{cladding} (the cladding pressure is dependent on the draw tension). For any given draw the only remaining control parameters are the furnace peak temperature and the relative core pressure, $\Delta P_{\text{core}} = P_{\text{core}} - P_{\text{cladding}}$; these two parameters are adjusted to target a draw tension of 400g and (when possible) a core size of 1/3 of the cladding diameter, respectively. The chosen draw tension produces the same stress as a solid fiber of 125μm OD drawn at 280g, which is a little higher but not too dissimilar from modern production draws of solid fibers which use tensions ranging from 100g to 250g (simulated production scale value calculated on uncoated fiber [12], and production scale experimental value measured on coated fiber [13] respectively).

The design considered here is based on a stack and draw of circular tubes producing a hexagonal lattice, other band-gap designs can be made using a square or triangular lattice. The dynamics of such designs will not be considered here, although we expect them to behave in a similar way as they are all made up from a lattice of small cladding holes and a larger core hole. Alternatives to stack and draw include extrusion, or drilling; regardless of how the preform is produced, however, all preforms are drawn to fiber in a similar way and will encounter the same dynamics as are considered here.

Table 1 shows the dimension and draw speed of the 12 preforms studied, while Fig. 2 shows the final structures of the simulated fibers drawn from 6 of the preforms defined in Table 1. For the fiber yields up to 50 km the target core size can be obtained, Fig. 2(b)–2(d). For $>$50 km yield the simulations indicate that the core would tend to collapse at mid-furnace, causing aborted draws. Increasing the core pressure can avoid this, but it results in larger cores and non-uniform cladding. Figure 2(e)–2(g) shows the smallest core we could achieve for the same targeted ID and OD for fiber yields of 100, 200 and 500 km. For the 100 km fiber the distortion

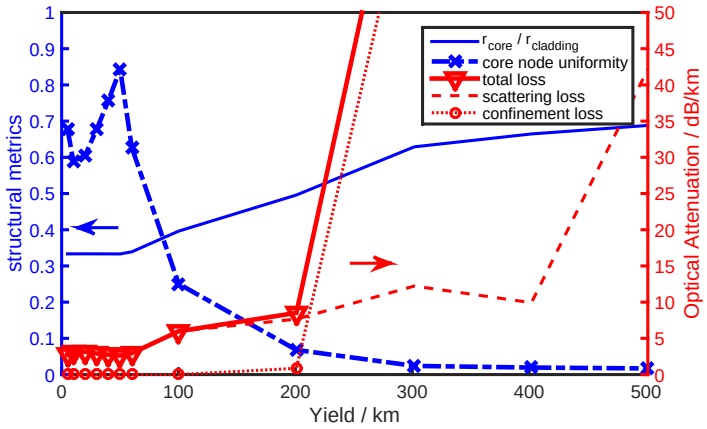

Fig. 3. The structural and optical attenuation properties for each of the different yield fibers: core size, $\phi_c = r_{\text{core}}/r_{\text{cladding}}$, and the uniformity of the core struts, $\phi_n = 1 - [\max(l) - \min(l)]/\max(l)$.

(larger corner holes and overall core) is already evident although somewhat controlled Fig. 2(e); beyond, 200 km Fig. 2(f) and 500 km fiber Fig. 2(g), it becomes extremely severe.

To describe key parts of the fiber structure we define two metrics: core size as a ratio of core radius to cladding radius $\phi_c = r_{\text{core}}/r_{\text{cladding}}$, and core node uniformity defined as $\phi_n = 1 - [\max(l) - \min(l)]/\max(l)$ where l is the distance between neighboring nodes around the core.

Figure 3 shows the core size and uniformity of the core region for each of the yields from Table 1. The yields $<$60 km show a high level of uniformity and the ability to control the core at the targeted 33%, while beyond that the core size increases and the core node uniformity drops. It has been already shown that a high core node uniformity is key to minimize the field overlap with the membranes and thus to reduce the surface scattering loss in the fiber [17]; a larger core size is expected to slightly reduce the surface scattering loss, however, it can also lead to a dramatic increase in confinement loss due to the compression of the holey cladding around the core. Figure 3 reports both of these loss components for each of the simulated fibers, obtained through finite element method (FEM) simulations of the structures obtained by the MSEM. The procedure to assign a suitable mass to the nodes can be found in [18]. It is clear that when the target core size is reached and the uniformity is reasonable the losses stay low ($\approx$3-4 dB/km), with a slight decrease at the highest core node uniformity. As the uniformity drops and the core size increases both the scattering and confinement losses increase. For yields $>$200 km the confinement loss dominates and the loss rapidly increases.

This exploration of longer yield draws has thus revealed a limiting issue; namely, it is difficult to maintain a small core size as the preform is enlarged. In the following sections we will explain how draw tension can be managed when increasing the preform size, how the dynamics of pressure and surface tension change the core size during the draw-down and how the relationship between the two changes depending on the preform size.

3.1. Upscaling challenge 1: managing draw stress

In this section we describe the changes required to the draw parameters in order to draw all the preform sizes with the same draw stress. We consider draw stress here, rather than draw tension, to extend generality to fibers of different sizes. The draw tension is sampled only at the

end of the neckdown where the fiber dimensions are close to convergence and the draw stress is highest. We will show here that higher draw stresses produce more uniform structures, however, if the stress is too high one increases the chance of fiber breaks during the draw; we therefore use a high, yet practical, draw stress value (222 MPa). To relate the draw parameters to the draw stress let us first consider the draw speed which can be determined from mass continuity, given by Eq. (1);

$$\left(R_2^2 - R_1^2\right) u_f = \left(r_2^2 - r_1^2\right) u_d \tag{1}$$

where R_1 and R_2 are the inner and outer radii of the jacket glass in the preform, and r for the fiber, u_f is the feed speed of the preform into the furnace, and u_d is fiber draw speed. It is obvious from Eq. (1) that larger preforms, R, fed at the same rate, u_f, which target the same final fiber, r, will require faster draw speeds, u_d.

Now consider the longitudinal draw stress, given by Eq. (2); here, for simplicity, we consider only the dominant viscous contribution, a more complete expression for draw stress including gravitational, inertial and surface tension terms can be found, for example, in [11].

$$\sigma_{zz} = 3\mu \mathrm{d}u/\mathrm{d}z \tag{2}$$

Where μ is the viscosity of the glass, u is the longitudinal velocity and z is the spatial coordinate in the longitudinal direction. The larger preforms require greater draw speeds, this results in a larger $\mathrm{d}u/\mathrm{d}z$. From Eq. (2) an increase in $\mathrm{d}u/\mathrm{d}z$ increases the draw stress, but too high a draw stress leads to an increased likelihood of fiber breaks; thus steps must be taken to maintain the draw stress at a safe level.

Considering Eq. (2), and continuing to target the same fiber, one has several options to draw larger preform sizes at the same draw stresses. One could reduce the feed speed, thereby reducing $\mathrm{d}u$, but while this is possible it is counterproductive as this will slow the rate of fiber production. Two alternative strategies remain:

1. Increase the temperature, to reduce the viscosity, μ.
2. Increase the length of the hot zone, increase $\mathrm{d}z$.

To quantify the impact that changing these two parameters has on the draw tension we simulated more than a hundred fiber draws in a 2D parameter sweep that covered a range of furnace lengths from 5 to 50 cm and furnace peak temperatures spanning 250 °C, with all other critical parameters (OD, ID, u_f, u_d) fixed (ΔP_{core} does not effect the draw stress of the fiber but must be changed for each tension to achieve the desired core size - discussed in Section 3.2). The resultant draw tension is shown in Fig. 4, where one can see that increasing the furnace length from 5 to 50 cm allows a reduction in peak temperature of ≈150 °C, for the same draw tension.

Several fibers along each of the 200g, 400g and 800g iso-tension lines were isolated and their microstructures examined: all structures on the same iso-tension line were found to be identical to the example structures in Fig. 4. Two similar studies conducted by changing feed speed with peak temperature, and considering uniform and Gaussian temperature profiles (results not included here) reached the same conclusion: in HC-PBGF draws the draw tension is the main control parameter for the microstructure. The same fibers can be obtained at a different peak temperature, furnace profile and/or feed speed, provided that the tension is maintained constant. This reflects the results of Chen and Birks [19] who found that tension was the driving parameter in their analytical and experimental study using only isolated holes in a drawn rod of glass, and the purely analytical study by Stokes et al. [20] for any arbitrary cross section. A different, but not unrelated, experimental study [21] found a similar conclusion for solid fibers, where the residual stress profiles are only dependent on draw tension rather than draw speed or temperature.

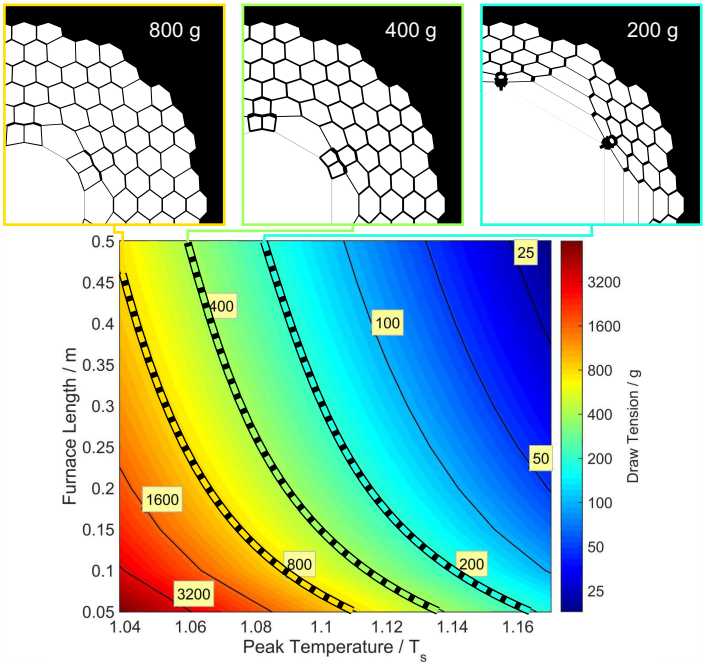

Fig. 4. Contours of draw tension for simulated draws with various furnace lengths and peak temperatures, T_s=1900K. Example structures on the iso-tension lines at 800 g, 400 g and 200 g Tension, all fibers along an iso-tension line were found to be exactly the same; ΔP_{core} was adjusted to give the best core size achievable: $\Delta P_{\text{core}}(800\text{g}) = -2900$ Pa, $\Delta P_{\text{core}}(400\text{g}) = -3800$ Pa, $\Delta P_{\text{core}}(200\text{g}) = -1730$ Pa.

Figure 4 shows simulation results of the 100 km fiber drawn at 3 tensions, core collapse mid-draw prevented the 100km fiber from being drawn with the target core size at 400g but clearly a tension of 800g allows the 100 km yield fiber to achieve the desired core size; when the tension is lowered to 200g the distortion is much more severe. It is desirable to draw at the highest tension possible as drawing at a higher tension allows for a more uniform structure.

The primary focus of this work is the structural impact of the thermodynamic parameters on the hollow microstructure, however, studies of solid fibers reveal additional considerations regarding the temperature and tension of the draw: fiber strength in service is drastically reduced if fiber is drawn at too high a tension [22, 23] while lower drawing temperatures have been shown to reduce the Rayleigh scattering coefficient [11, 24].

In conclusion we have shown that higher draw stress allows for more uniform structures to be drawn, but this is constrained by the increased likelihood of fiber breaks at high stress. When increasing the preform size the draw tension, Eq. (2), can be kept constant by increasing the furnace length or peak furnace temperature (between the lower and upper limits of the softening and boiling point of silica). Regardless of how the furnace is changed if the tension is the same the microstructure of the final fiber will be the same.

3.2. Upscaling challenge 2: managing core size

During the draw of a simple glass tube the surface tension acting on the inner surface will generate a pressure on the surface, P_{st}, given by Eq. (3), which will tend to collapse it; to

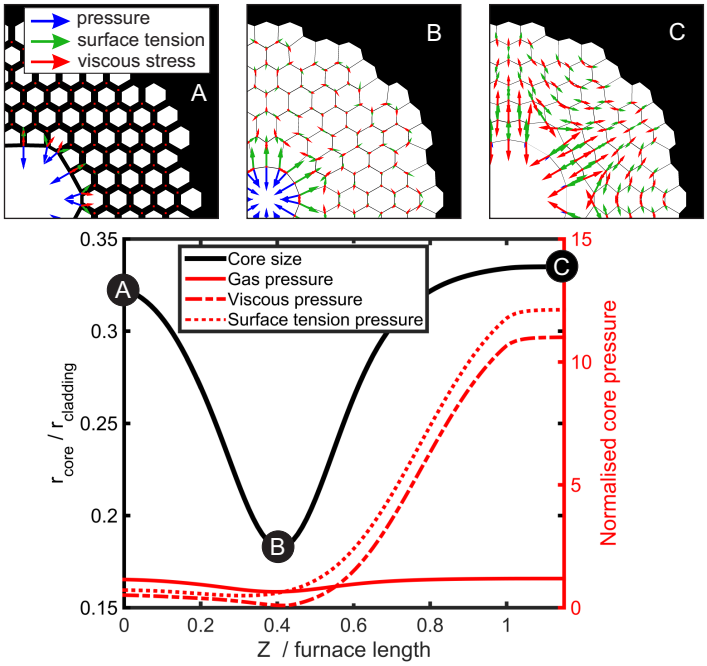

Fig. 5. The change in $r_{\text{core}}/r_{\text{cladding}}$ and the magnitude of the radial pressures around the core during the draw. ΔP_{core} acts in the opposite direction to the surface tension. The pressure applied has been chosen to achieve a $r_{\text{core}}/r_{\text{cladding}} = 1/3$ in the final fiber. Force vectors in the microstructure are shown at 3 distinct stages in the draw down, A, B, C.

prevent hole collapse a positive gas pressure in the tube must be applied.

$$P_{\text{st}} = \gamma / R_{\text{hole}} \tag{3}$$

where γ is the surface tension property of the material and R_{hole} is the radius of the hole. In HC-PBGFs the relationship is similar but since these fibers contain hundreds of holes, each hole will have a surface tension pressure acting on it. The equal sized cladding holes and the larger core hole behave rather differently, each being subject to a different surface tension: the one associated with the core radius would cause the core to contract, if not counterbalanced by the stronger one associated with the cladding hole radii, which causes each of the cladding holes to collapse, and as a result the core to expand. The difference in radii of these two groups is such that to maintain the core ratio of the original preform a larger gas pressure must be applied to the cladding holes, and a smaller gas pressure must be applied to the core. To achieve a certain fiber ID one must apply a specific cladding pressure P_{cladding}; the core size is therefore controlled by the difference between the core and cladding pressures defined as $\Delta P_{\text{core}} = P_{\text{core}} - P_{\text{cladding}}$, where a larger ΔP_{core} results in a larger core.

During the draw the cross-sectional geometry undergoes a dramatic reduction in size. The pressure due to surface tension is a function of $1/R_{\text{hole}}$, Eq. (3), and increases as the hole becomes smaller. However, the applied gas pressure, ΔP_{core}, is constant (to first approximation) and acts equally throughout the neck-down. As the fiber is drawn down the difference between P_{st} and ΔP_{core} will therefore change. Typically, at the start of the draw the applied differential gas pressure is of greater magnitude than the surface tension, this forces the core to contract relative to the surrounding microstructure, Fig. 5. Then, as the fiber is drawn down and the whole

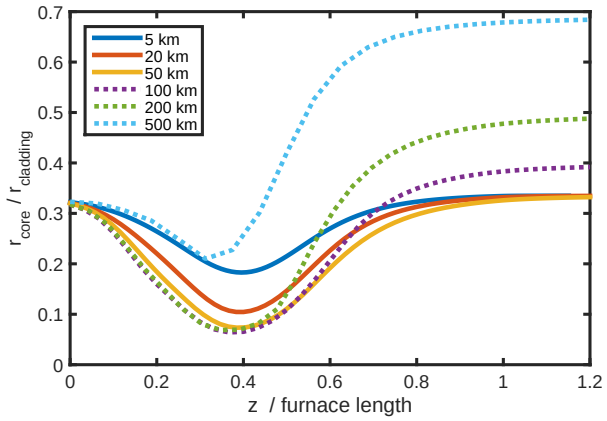

Fig. 6. Core size during draw for a selection of preform sizes, dashed lines indicate cases with cores that are too large.

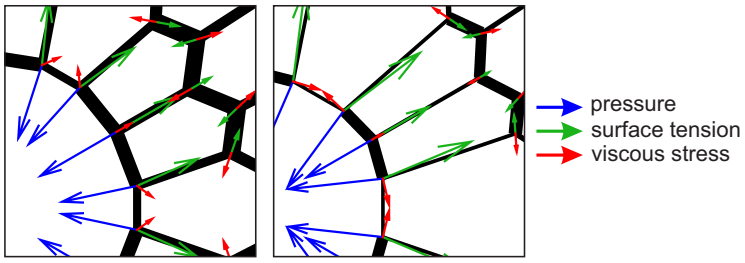

Fig. 7. Force vector plots of the core surround at z/L = 8% (left) and 9% (right) during the 500 km fiber draw. The plots highlight a second distortion dynamic that can occur during the contraction phase. The misalignment between negative core pressure (blue) and positive surface tension (green) causes the core strut of the corner holes to become thin and long compared to the other core surrounding struts.

structure becomes smaller, the surface tension contribution increases and eventually becomes larger than the gas pressure, causing the core to enlarge again. Choosing the correct gas pressure allows the final fiber core to reach the desired size, Fig. 5.

However, in order to keep the draw tension constant (close to the maximum possible value to avoid breaks), as the preform size is increased measures are taken (e.g. reducing viscosity) that cause the radial stiffness of the microstructure to decrease. This in turn allows the surface tension to impact greater changes in the latter half of the draw, resulting in a larger core in the final fiber, Fig. 6. To counter the increased core size the core gas pressure must be lowered. In the cases we examined, this became a limiting factor for the 60 km fiber and above. We observed that if the core contracted beyond a certain point ($\approx$8% of the cladding radius) the structure could not recover due to some of the core surrounding nodes coalescing together. Therefore, in order to successfully draw the $>$60 km fibers we had to apply less core pressure, producing fibers with a core that was larger than the target, with consequent structural distortions that led to a higher overall loss, see the three longest yields in Fig. 6 and the loss in Fig. 3. Note that in our numerical model core collapse makes convergence very difficult because components of the geometry become singular; this is equivalent to behaviour in experimental draws in which the core can become misshapen or elliptical and nodes can coalesce, disrupting the periodicity of the structure and greatly increasing the loss.

The 500 km case displays an additional distortion dynamic in the core-surrounding cells, occuring before the minimum contraction point. Figure 7 shows that there is a rapid change in size of the core strut associated with the corner holes. The surface tension and core pressure are not aligned, which causes the stretching of the strut. For the lower yields this change is countered by the viscous force before large non-uniformities can occur. But the measures taken to maintain 'safe' draw tension in the 500 km yield fiber cause the viscous resistance of that strut to be insufficient to prevent this distortion. This occurs before the point of minimum contraction highlighted by Fig. 6. We believe this distortion mechanism is always present, to some degree, in all the draws performed here and is responsible for the variation in node spacing around the core. However, it becomes strikingly evident only in the most extreme cases.

4. Conclusion

We have used fiber draw simulations to investigate for the first time how to increase the yield of HC-PBGFs from the several km lengths currently produced in the laboratory to the much longer lengths required for mass producing such fibers, and we have highlighted the problems, unique to this fiber technology, that one would encounter and would need to address. For the preform design investigated here, corresponding to a fabricated fiber of $\approx$11 km, we have found that for up to 60 km no substantial modifications to the current draw process would be required; the 100 km yield however already has some distortion leading to loss increase, while beyond that the distortions are severe. To increase the yield further beyond this point several strategies are possible: longer preforms (2-3 m is not uncommon in the commercial setting) will give a proportional increase in yield but no increase in production rate (though this will reduce the time spent swapping out preforms and setting up the draw). Additionally, use of a higher draw tension or microstructure stiffness can make longer yields achievable before the core-size issues identified here occur. A possible way to stiffen the microstructure (without changing the draw stress) is to increase the relative strut thickness in the preform and in the targeted final fiber, at the cost of decreasing the air filling fraction and consequently altering the final optical properties of the fiber. Finally, in addition to all these strategies, selective cell pressurization can also be applied to prevent some core surround holes from becoming too large or too small. While this would not directly prevent the core from becoming too large, it could improve uniformity in the core surround and thus reduce the loss. By combining all these strategies, we believe that final fiber yields in the range of 300-500 km per preform should ultimately be a realistic target.

This work has also furthered the understanding of the draw dynamics of hollow core microstructured fibers. We have found that draw tension is the driving parameter controlling the microstructure, rather than peak temperature, furnace profile or preform feed rate - which, from a structural point of view, are all equivalent. We have identified changes in the ratio between surface tension and gas pressure at different points during the neck-down resulting in an initial contraction and then expansion of the core, and that this contraction presents a limit to the minimum achievable core size. We have also highlighted a second type of distortion that becomes dominant in the longest yield fibers, but which is present in all, and is associated with the large corner holes observed in many reported fibers. The draw simulations performed in this study all produce fiber with the same dimensions, however, the analysis of Sections 3.1 and 3.2 are generalizable to all fiber dimensions and materials. We believe the study shines new light into the drawing dynamics of HC-PBGFs and it can prove a valuable contribution to the development of longer yield fibers.

Acknowledgments

This work was supported by the EU 7th Framework Programme under grant agreement 258033 (MODE-GAP), and by the UK EPSRC through grant EP/I01196X/1 (HYPERHIGHWAY) and

EP/H02607X/1 (EPSRC Centre for Innovative Manufacturing in Photonics). FP and DJR gratefully acknowledge support from the Royal Society. The authors acknowledge the use of the IRIDIS High Performance Computing Facility, and associated support services at the University of Southampton, in the completion of this work. Data supporting this study are openly available from the University of Southampton repository at http://dx.doi.org/10.5258/SOTON/377858.